Journal of Materials Chemistry A

ROYAL SOCIETY OF CHEMISTRY

COMMUNICATION

View Article Online
View Journal | View Issue

Cite this: J. Mater. Chem. A, 2023, 11, 6814

Received 2nd February 2023
Accepted 3rd March 2023

DOI: 10.1039/d3ta00606a

rsc.li/materials-a

Main-group indium single-atom catalysts for electrocatalytic NO reduction to NH_3†

Kai Chen,‡ Nana Zhang,‡ Fuzhou Wang, Jilong Kang and Ke Chu *

Main-group metal elements show great potential for exploring high-performance catalysts for electrochemical reduction of NO to NH_3 (NORR) but remain largely unexplored. Herein, as a proof-of-concept, main-group In single atoms confined in an amorphous MoO_3 substrate (In_1/a-MoO_3) are explored as an efficient NORR catalyst, showing a maximum NH_3 yield of 242.6 μmol h^{-1} cm^{-2} and NH_3-faradaic efficiency of 92.8%. Further experiments and theoretical results identify single-site In atoms as the dominating active centers to simultaneously inhibit the hydrogen evolution and optimize the hydrogenation energetics of the NO-to-NH_3 pathway.

Ammonia is a critical industrial chemical which is widely used in modern economic development.[1–3] Electrochemical N_2 fixation through N_2 electroreduction (NRR) enables sustainable NH_3 synthesis under ambient conditions with near-zero CO_2 emissions.[4–8] Unfortunately, the NRR is still far from being practicable on account of the competitive hydrogen evolution reaction (HER) and ultrastrong N≡N bond.[9–15]

Compared with the NRR, electrochemical NO-to-NH_3 conversion (NORR) is a more energy-efficient and practically feasible approach for sustainable NH_3 synthesis.[16–21] Meanwhile, NO is one of the common atmospheric pollutants, arising from vehicle exhaust emissions and insufficient combustion of fossil fuels.[18] Therefore, the NORR represents a fascinating method for realizing both detrimental NO treatment and effective NH_3 electrosynthesis.[18] Nevertheless, the NORR is a multi-step process involving a complex five-electron process and hindered by the competing HER.[22–25] Therefore, exploring high-performance catalysts to achieve both NORR promotion and HER inhibition is urgently demanded.

Diverse transition metal-based materials have been reported as active NORR catalysts,[26–29] by virtue of their partially occupied d-orbitals to enhance NO adsorption and dissociation. Nonetheless, d-orbitals also contribute to *H binding on the catalyst surface, which is beneficial for the competitive HER and unfavorable for FE_{NH_3}.[30] Alternatively, main-group metals, such as In, Sn, Sb and In, with partially occupied p-orbitals but an intrinsic characteristic of poor *H binding, have attracted growing attention for selective NH_3 electrosynthesis.[31–36] On the other hand, single atom catalysts (SACs) with isolated metal sites have been extensively demonstrated to exhibit superior properties for various electrocatalytic reactions owing to their maximized atomic utilization and unique coordination configuration.[37–42] Inspired by the above, main-group SACs may hold great promise toward the active and selective NORR.

In this study, as a proof-of-concept, we first explore main-group In single atoms confined in amorphous MoO_3 (In_1/a-MoO_3) as an effective NORR catalyst, which exhibits a maximum FE_{NH_3} of 92.8% and NH_3 yield rate of 242.6 μmol h^{-1} cm^{-2}. Detailed experiments and computational studies are performed to elucidate the origin for the exceptional NORR properties of In_1/a-MoO_3.

In_1/a-MoO_3 was prepared by a facile supercritical CO_2 approach.[43–45] The characteristic transmission electron microscopy (TEM, Fig. 1a) image of In_1/a-MoO_3 presents a nanosheet morphology, while the high-resolution TEM (HRTEM, Fig. 1b) image shows no obvious lattice fringes, similar to bare a-MoO_3 (Fig. S1†). The corresponding fast Fourier transform (FFT, Fig. 1c) pattern unravels a sun-like feature, consistent with the lunar halo displayed in the selected area electron diffraction (SAED, Fig. S2†) pattern. Additionally, no noticeable diffraction peaks can be seen in the X-ray diffraction (XRD, Fig. 1d) pattern. All these HRTEM/FFT/SAED/XRD results confirm the amorphous structure of In_1/a-MoO_3. In the aberration-corrected high angle annular dark-field scanning transmission electron microscopy (AC-HAADF-STEM) image (Fig. 1e), there are numerous bright points (marked by red circles) that are highly dispersed on the amorphous substrate, and this can be further unveiled by the 3D intensity profile (Fig. 1f), proving that In species are atomically dispersed on a-MoO_3. Elemental

School of Materials Science and Engineering, Lanzhou Jiaotong University, Lanzhou 730070, China. E-mail: chuk630@mail.lzjtu.cn

† Electronic supplementary information (ESI) available. See DOI: https://doi.org/10.1039/d3ta00606a

‡ These authors contributed equally to this work.

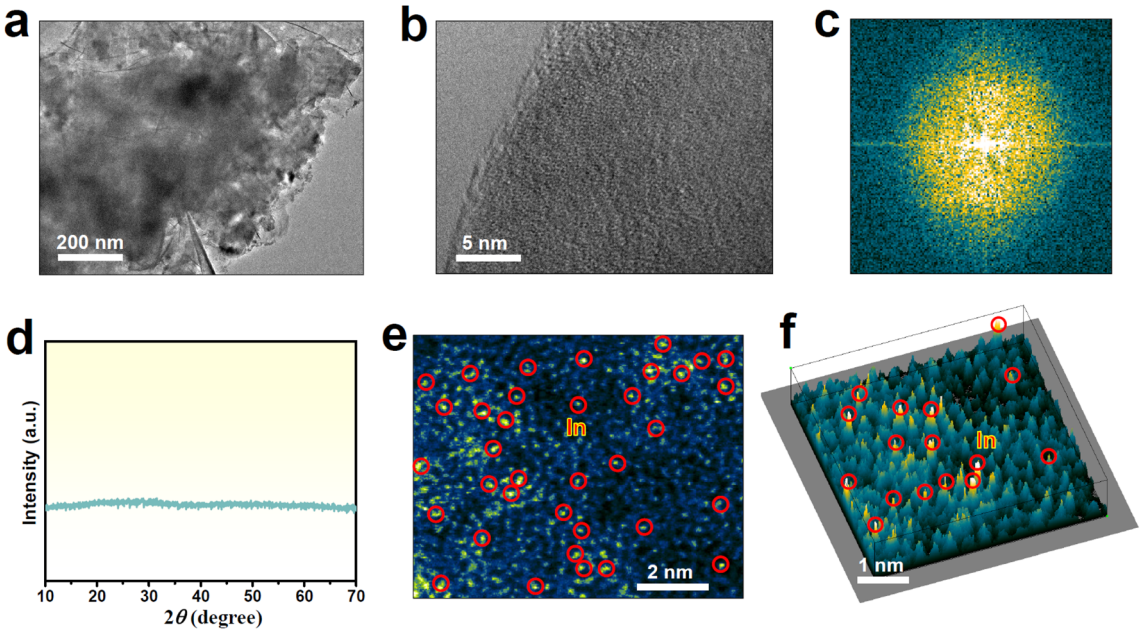

Fig. 1 Characterization of In_1/a-MoO_3: (a) TEM image, (b) HRTEM image and corresponding FFT pattern (c), (d) XRD pattern, (e) AC-HAADF-STEM image and corresponding (f) 3D intensity profile.

mapping images (Fig. S3†) display an even distribution of In single atoms over the a-MoO_3 support. The In content in In_1/a-MoO_3 is measured to be as high as 8.2 wt%, much higher than that of reported In single atoms on carbon substrates.[40,46,47]

The valence states and local atomic coordination structure of In_1/a-MoO_3 are studied by X-ray absorption fine structure (XAFS) analyses. The In K-edge X-ray absorption near-edge structure (XANES) spectra show that the absorption edge of In_1/a-MoO_3 (Fig. 2a) lies between In foil and In_2O_3 references, indicating that In single atoms are in a positive valence state.[48] In the In K-edge extended X-ray adsorption fine structure (EXAFS) spectra (Fig. 2b), In_1/a-MoO_3 shows a distinct peak located at 1.61 Å, which is ascribed to the In–O coordination bond. The absence of the In–In coordination bond (2.97 Å) indicates that In presents as an isolated atomic state,[49–52] consistent with the AC-HAADF-STEM observation (Fig. 1e). Meanwhile, unlike the In_2O_3 reference, no second-shell In–O–In bond (3.09 Å) shows up in In_1/a-MoO_3, excluding the existence of In_2O_3 species on

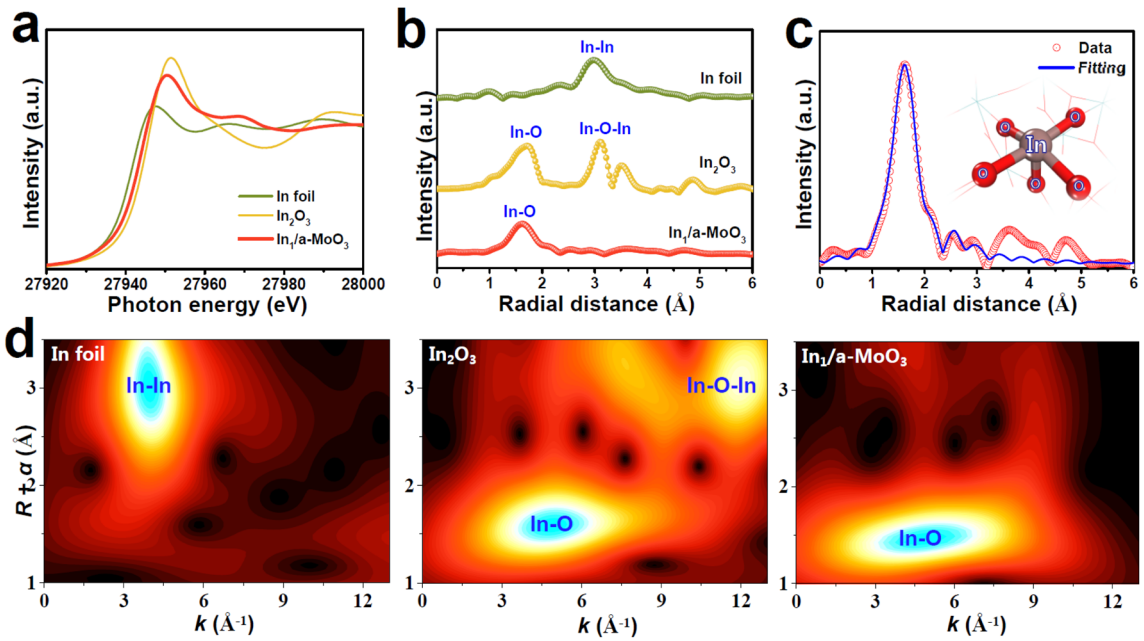

Fig. 2 (a) In K-edge XANES, (b) EXAFS spectra and (d) WT pattern of In_1/a-MoO_3 and reference samples. (c) EXAFS fitting curve of In_1/a-MoO_3 (inset: fitting model).

In_1/a-MoO_3. These EXAFS findings can be further corroborated by wavelet transform (WT) analysis (Fig. 2d), revealing that In_1/a-MoO_3 exhibits the solo In–O maximum intensity with no presence of In–In/In–O–In WT signals. Quantitative EXAFS fitting of In_1/a-MoO_3 (Fig. 2c and S4†) uncovers that single-site In is coordinated with five O atoms to form an In_1–O_5 motif. Moreover, *ab initio* molecular dynamic (AIMD, Fig. S5†) simulations reveal that the In_1–O_5 motif can well maintain the equilibrium temperature/energy states at temperature as high as 500 K, confirming the high thermodynamic stability of the In_1–O_5 motif, which is attributed to the strong In_1–O_5 electronic coupling to well stabilize In single atoms on the a-MoO_3 substrate (Fig. S6†).

The electrocatalytic NORR properties of In_1/a-MoO_3 are assessed in a gas-tight H-type cell with 0.5 M Na_2SO_4.[29] Colorimetric methods are used to detect the liquid reduction products (Fig. S7 and S8†), while gas products are detected by gas chromatography. To initially assess the NORR activity of In_1/a-MoO_3, we perform linear sweep voltammetry (LSV) measurements (Fig. 3a). A remarkable current density (j) enhancement can be observed in NO-solution relative to Ar-solution, verifying a good electrocatalytic NORR ability of In_1/a-MoO_3. We then quantify the NORR performance of In_1/a-MoO_3 at various potentials through combined chronoamperometry (Fig. 3b) and colorimetric methods. As shown in Fig. 3c, with increasing the potentials, In_1/a-MoO_3 shows a volcano-type variation in both the NH_3 yield rate and FE_{NH_3}, attaining their highest values of 242.6 μmol h^{-1} cm^{-2} and 92.8% at −0.6 V, respectively, which are higher than those of nearly all previously reported catalysts (Fig. 3d, Table S2†). Strikingly, In_1/a-MoO_3 drastically outperforms bare a-MoO_3 in both the NH_3 yield rate and FE_{NH_3} (Fig. S9 and S10†), suggesting that single-atomic In introduction plays a pivotal role in greatly boosting the NORR performance. The significant reduction of the NH_3 yield rate and FE_{NH_3} at −0.7 V is due to the enhancement in the competing HER process (Fig. 3e). Meanwhile, Fig. 3e shows that the FE_{NH_3} of In_1/a-MoO_3 is much higher than the FEs of other nitrogen-containing N_2 and N_2H_4 by-products, in accordance with the partial current density data (Fig. S11†), indicating that In_1/a-MoO_3 has an exceptional NORR selectivity for NO-to-NH_3 conversion. The NORR stability of In_1/a-MoO_3 is assessed by 15 h of continuous electrolysis (Fig. S12†), which shows that the current density is rather steady and the corresponding FE_{NH_3} does not show remarkable changes, suggesting that In_1/a-MoO_3 has good long-term stability. Besides, during seven electrolysis cycles (Fig. 3f), the resulting NH_3 yield rates and FE_{NH_3} only slightly fluctuate, proving the excellent cycling stability of In_1/a-MoO_3.[53] After the stability test, In_1/a-MoO_3 well retains its nanosheet morphology, amorphous structure and atomic Ir dispersion state (Fig. S13†), demonstrating that the surface reconstruction of In_1/a-MoO_3 barely occurs and thus In_1/a-MoO_3 possesses high structural stability. Furthermore, the control colorimetric test (Fig. S14†), Ar–NO alternating cycle test (Fig. S15†), and ^1H nuclear magnetic resonance test (NMR, Fig. S16†) prove that the generated NH_3 comes from the NORR process.

Theoretical computations are carried out to shed light on the NORR mechanism of In_1/a-MoO_3. Based on the EXAFS fitting result (Fig. 2c), an isolated In_1–O_5 motif constructed on a-MoO_3 is employed to simulate In_1/a-MoO_3. Upon the adsorption of NO on the In site, the charge density difference map (Fig. 4a) depicts a considerable *NO/In electronic interaction. Notably, *NO shows pronounced positive charge accumulation, implying that the In site can effectively activate the NO molecule through a "σ-donation" mechanism. Prior to assessing the hydrogenation energetics of the NORR pathway, we conduct online differential electrochemical mass spectrometry (DEMS) to monitor the key intermediates and determine the optimal reaction path on In_1/a-MoO_3. Fig. 4b displays the absence of the

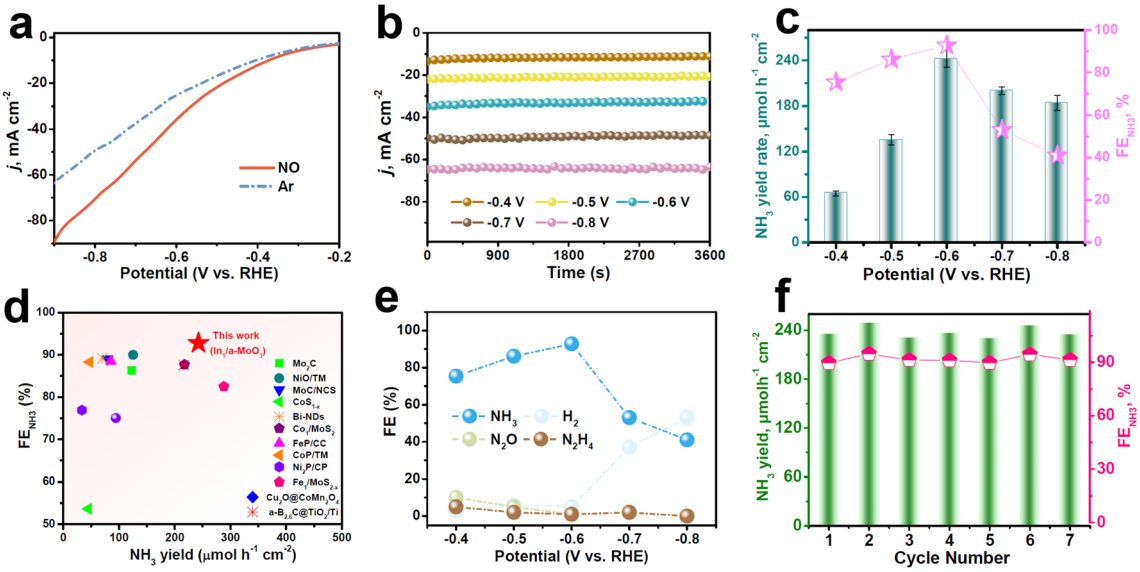

Fig. 3 (a) LSV curves of In_1/a-MoO_3 in Ar/NO-saturated 0.5 M Na_2SO_4 at a rate of 10 mV s^{-1}. (b) Chronoamperometry test of In_1/a-MoO_3 at various potentials, and resulting (c) NH_3 yield rates and FE_{NH_3}. (d) Comparison of NH_3 yields and FE_{NH_3} between In_1/a-MoO_3 and reported NORR catalysts. (e) FEs of different products on In_1/a-MoO_3 after NORR electrolysis at various potentials. (f) Cycling test of In_1/a-MoO_3 at −0.6 V.

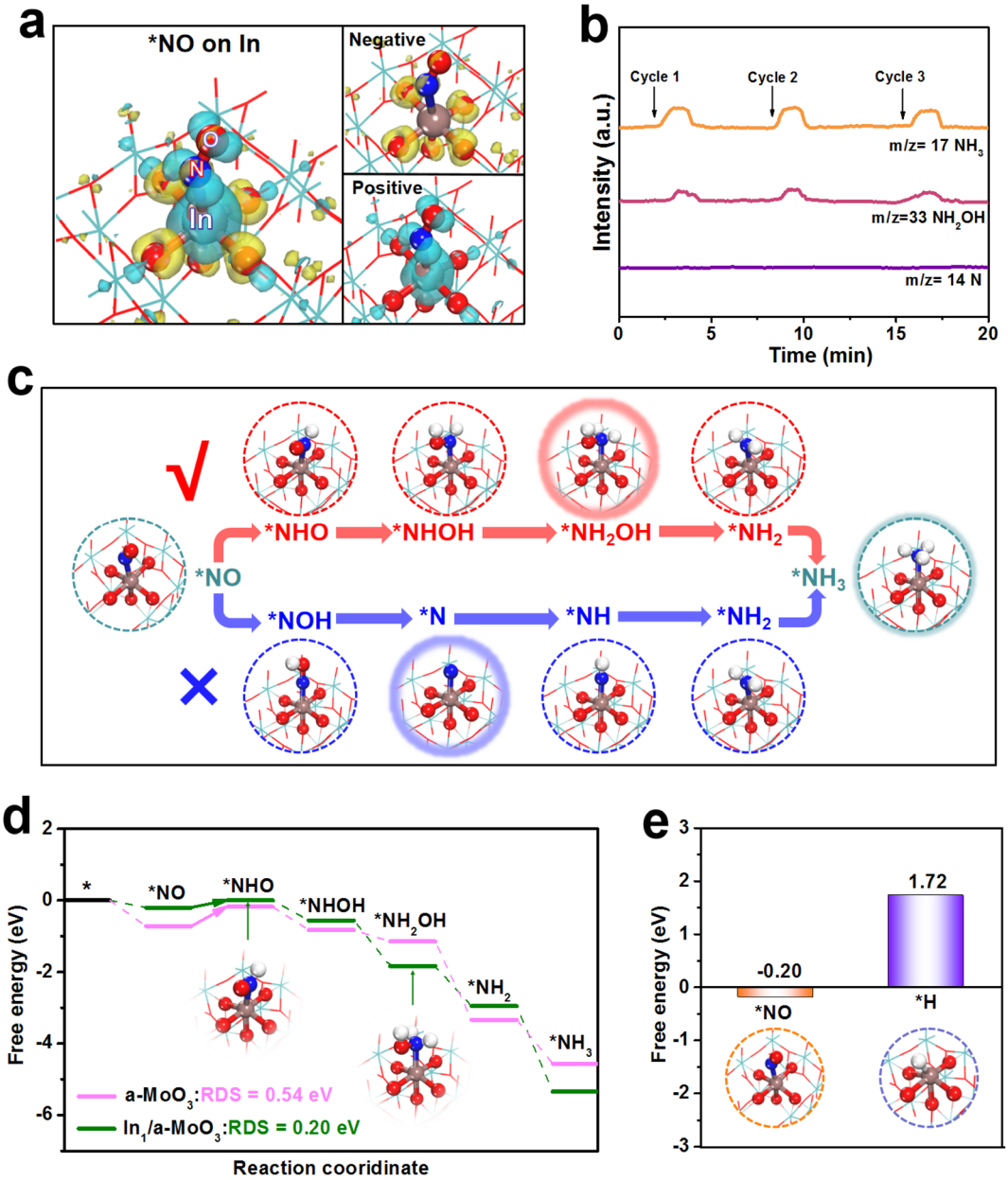

Fig. 4 (a) Charge density difference of absorbed NO (*NO) on In_1/a-MoO_3. Yellow and cayan regions represent electron depletion and accumulation, respectively. (b) Online DEMS spectra of In_1/a-MoO_3 during the electrolysis at −0.6 V. (c) Schematic of typical NOH and NHO pathways on In_1/a-MoO_3. (d) Free energy profiles of the NORR process (NHO pathway) on the Mo site (a-MoO_3) and In site (In_1/a-MoO_3). (e) Binding free energies of *NO and *H on the In site of In_1/a-MoO_3.

N intermediate but the presence of the NH_2OH intermediate, implying that In_1/a-MoO_3 prefers to adopt a NHO pathway (*NO → *NHO → *NHOH → *NH_2OH → *NH_2 → *NH_3) rather than a NOH pathway (*NO → *NOH → *N → *NH → *NH_2 → *NH_3) to drive the NORR process (Fig. S17†),[54,55] as illustrated in Fig. 4c. As shown in the free energy diagrams along the NHO pathway (Fig. 4d), the In site presents the initial *NO protonation (*NO → *NHO) as the rate-determining step (RDS) with a low energy barrier of 0.20 eV. As a sharp comparison, the Mo site of bare a-MoO_3 shows the same *NO → *NHO as the RDS, but exhibits a largely increased RDS barrier of 0.54 eV due to too strong *NO binding on the Mo site. Thus, single-site In can effectively optimize the binding energy of *NO to reduce the RDS barrier, thereby significantly promoting the hydrogenation energetics of the NO-to-NH_3 pathway.

As the HER is regarded as the major competitive reaction against the NORR,[56–62] we further evaluate the HER activity of In_1/a-MoO_3. Fig. 4e shows that the binding free energy of *H (1.72 eV) on the In site is much more positive than that of *NO (−0.20 eV), proving that the In site can favorably absorb NO while restricting H binding. In the molecular dynamics (MD) simulations (Fig. S18†), *NO/In interaction is found to be much stronger than *NO/In interaction after simulations, as evidenced by the radial distribution function (RDF, Fig. S19†)

curves and integrated RDF curves (Fig. S20†), verifying the priority of In_1/a-MoO_3 for the absorption and coverage of NO over H.[63–66] Therefore, in addition to promoting the NO hydrogenation energetics, single-site In can facilitate HER suppression to enable the achievement of a high NORR selectivity.

In summary, In_1/a-MoO_3 is validated as an effective NORR catalyst. As unraveled by the experimental measurements and theoretical calculations, the prominent NORR properties of In_1/a-MoO_3 are attributed to the ability of single-site In to inhibit the HER and boost the hydrogenation energetics of the NO-to-NH_3 pathway. This work would open a new avenue for the development of efficient main-group SACs for high-performance NORR electrocatalysis.

Conflicts of interest

There are no conflicts of interest to declare.

Acknowledgements

This work is supported by the Central Government Guides Local Science and Technology Development Project (206Z1003G) and Fundamental Researches Top Talent Program of Lanzhou Jiaotong University (2022JC03).

References

1 J. Liang, Q. Liu, A. A. Alshehri and X. Sun, *Nano Res. Energy*, 2022, **1**, e9120010.
2 D. Qi, F. Lv, T. Wei, M. Jin, G. Meng, S. Zhang, Q. Liu, W. Liu, D. Ma, M. S. Hamdy, J. Luo and X. Liu, *Nano Res. Energy*, 2022, **1**, e9120022.
3 G. Qing, R. Ghazfar, S. T. Jackowski, F. Habibzadeh, M. M. Ashtiani, C.-P. Chen, M. R. Smith and T. W. Hamann, *Chem. Rev.*, 2020, **120**, 5437–5516.
4 X. Zhao, G. Hu, G. F. Chen, H. Zhang, S. Zhang and H. Wang, *Adv. Mater.*, 2021, **33**, 2007650.
5 K. Tanifuji and Y. Ohki, *Chem. Rev.*, 2020, **120**, 5194–5251.
6 K. Chu, X. Li, Q. Li, Y. Guo and H. Zhang, *Small*, 2021, **17**, 2102363.
7 X. Li, Y. Luo, Q. Li, Y. Guo and K. Chu, *J. Mater. Chem. A*, 2021, **9**, 15955–15962.
8 K. Chu, X. Li, Y. Tian, Q. Li and Y. Guo, *Energy Environ. Mater.*, 2022, **5**, 1303–1309.
9 C. Guo, J. Ran, A. Vasileff and S.-Z. Qiao, *Energy Environ. Sci.*, 2018, **11**, 45–56.
10 J. Deng, J. A. Iñiguez and C. Liu, *Joule*, 2018, **2**, 846–856.
11 X. Cui, C. Tang and Q. Zhang, *Adv. Energy Mater.*, 2018, **8**, 1800369.
12 Y. Luo, P. Shen, X. Li, Y. Guo and K. Chu, *Nano Res.*, 2022, **15**, 3991–3999.
13 Q. Li, P. Shen, Y. Tian, X. Li and K. Chu, *J. Colloid Interface Sci.*, 2022, **606**, 204–212.
14 K. Chu, J. Wang, Y. Liu, Q. Li and Y. Guo, *J. Mater. Chem. A*, 2020, **8**, 7117–7124.
15 M. Wang, S. Liu, T. Qian, J. Liu, J. Zhou, H. Ji, J. Xiong, J. Zhong and C. Yan, *Nat. Commun.*, 2019, **10**, 341.
16 J. Long, S. Chen, Y. Zhang, C. Guo, X. Fu, D. Deng and J. Xiao, *Angew. Chem., Int. Ed.*, 2020, **59**, 9711–9718.
17 S. Cheon, W. J. Kim, D. Y. Kim, Y. Kwon and J.-I. Han, *ACS Energy Lett.*, 2022, **7**, 958–965.
18 B. H. Ko, B. Hasa, H. Shin, Y. Zhao and F. Jiao, *J. Am. Chem. Soc.*, 2022, **144**, 1258–1266.
19 J. Wu and Y.-X. Yu, *J. Colloid Interface Sci.*, 2022, **623**, 432–444.
20 B. Huang, B. Chen, G. Zhu, J. Peng, P. Zhang, Y. Qian and N. Li, *ChemPhysChem*, 2022, **23**, e202100785.
21 Q. Wu, H. Wang, S. Shen, B. Huang, Y. Dai and Y. Ma, *J. Mater. Chem. A*, 2021, **9**, 5434–5441.
22 J. Liang, P. Liu, Q. Li, T. Li, L. Yue, Y. Luo, Q. Liu, N. Li, B. Tang, A. A. Alshehri, I. Shakir, P. O. Agboola, C. Sun and X. Sun, *Angew. Chem., Int. Ed.*, 2022, **61**, e202202087.
23 Y. Xiao and C. Shen, *Small*, 2021, **17**, 2100776.
24 K. Chen, G. Wang, Y. Guo, D. Ma and K. Chu, *Nano Res.*, 2023, DOI: **10.1007/s12274-023-5556-7**.
25 K. Chen, G. Zhang, X. Li, X. Zhao and K. Chu, *Nano Res.*, 2023, DOI: **10.1007/s12274-023-5384-9**.
26 K. Chen, P. Shen, N. Zhang, D. Ma and K. Chu, *Inorg. Chem.*, 2023, **62**, 653–658.
27 T. Wei, H. Bao, X. Wang, S. Zhang, Q. Liu, J. Luo and X. Liu, *ChemCatChem*, 2023, **15**, e202201411.
28 H. Zhang, Y. Li, C. Cheng, J. Zhou, P. Yin, H. Wu, Z. Liang, J. Zhang, Q. Yun and A. L. Wang, *Angew. Chem., Int. Ed.*, 2022, e202213351.
29 K. Chen, J. Wang, J. Kang, X. Lu, X. Zhao and K. Chu, *Appl. Catal., B*, 2023, **324**, 122241.
30 G. F. Chen, S. Y. Ren, L. L. Zhang, H. Cheng, Y. R. Luo, K. H. Zhu, L. X. Ding and H. H. Wang, *Small Methods*, 2019, **3**, 1800337.
31 Y. Wang, M. M. Shi, D. Bao, F. L. Meng, Q. Zhang, Y. T. Zhou, K. H. Liu, Y. Zhang, J. Z. Wang, Z. W. Chen, D. P. Liu, Z. Jiang, M. Luo, L. Gu, Q. H. Zhang, X. Z. Cao, Y. Yao, M. H. Shao, Y. Zhang, X. B. Zhang, J. G. Chen, J. M. Yan and Q. Jiang, *Angew. Chem., Int. Ed.*, 2019, **58**, 9464–9469.
32 Y. Sun, Y. Wang, H. Li, W. Zhang, X.-M. Song, D.-M. Feng, X. Sun, B. Jia, H. Mao and T. Ma, *J. Energy Chem.*, 2021, **62**, 51–70.
33 L. Li, C. Tang, H. Jin, K. Davey and S.-Z. Qiao, *Chem*, 2021, **7**, 3232–3255.
34 N. Zhang, J. Shang, X. Deng, L. Cai, R. Long, Y. Xiong and Y. Chai, *ACS Nano*, 2022, **16**, 4795–4804.
35 Y. Lin, J. Liang, H. Li, L. Zhang, T. Mou, T. Li, L. Yue, Y. Ji, Q. Liu, Y. Luo, N. Li, B. Tang, Q. Wu, M. S. Hamdy, D. Ma and X. Sun, *Mater. Today Phys.*, 2022, **22**, 100611.
36 X. Li, G. Zhang, P. Shen, X. Zhao and K. Chu, *Inorg. Chem. Front.*, 2023, **10**, 280–287.
37 L. Zhang, M. Zhou, A. Wang and T. Zhang, *Chem. Rev.*, 2019, **120**, 683–733.
38 S. K. Kaiser, Z. Chen, D. Faust Akl, S. Mitchell and J. Pérez-Ramírez, *Chem. Rev.*, 2020, **120**, 11703–11809.
39 R. Lang, X. Du, Y. Huang, X. Jiang, Q. Zhang, Y. Guo, K. Liu, B. Qiao, A. Wang and T. Zhang, *Chem. Rev.*, 2020, **120**, 11986–12043.

40 S. Li, X. Lu, S. Zhao, M. Ceccato, X.-M. Hu, A. Roldan, M. Liu and K. Daasbjerg, *ACS Catal.*, 2022, **12**, 7386–7395.
41 W. Guo, X. Tan, J. Bi, L. Xu, D. Yang, C. Chen, Q. Zhu, J. Ma, A. Tayal, J. Ma, Y. Huang, X. Sun, S. Liu and B. Han, *J. Am. Chem. Soc.*, 2021, **143**, 6877–6885.
42 F. Luo, A. Roy, L. Silvioli, D. A. Cullen, A. Zitolo, M. T. Sougrati, I. C. Oguz, T. Mineva, D. Teschner, S. Wagner, J. Wen, F. Dionigi, U. I. Kramm, J. Rossmeisl, F. Jaouen and P. Strasser, *Nat. Mater.*, 2020, **19**, 1215–1223.
43 K. Chen, Y. Zhang, J. Xiang, X. Zhao, X. Li and K. Chu, *ACS Energy Lett.*, 2023, **8**, 1281–1288.
44 Y. Luo, Q. Li, Y. Tian, Y. Liu and K. Chu, *J. Mater. Chem. A*, 2022, **10**, 1742–1749.
45 K. Chen, J. Wang, H. Zhang, D. Ma and K. Chu, *Nano Lett.*, 2023, **23**, 1735–1742.
46 E. Zhang, L. Tao, J. An, J. Zhang, L. Meng, X. Zheng, Y. Wang, N. Li, S. Du, J. Zhang and Y. Li, *Angew. Chem., Int. Ed.*, 2022, **134**, e202117347.
47 H. Shang, T. Wang, J. Pei, Z. Jiang, D. Zhou, Y. Wang, H. Li, J. Dong, Z. Zhuang, W. Chen, W. Dingsheng, J. Zhang and Y. Li, *Angew. Chem., Int. Ed.*, 2020, **59**, 22465–22469.
48 P. Shen, X. Li, Y. Luo, N. Zhang, X. Zhao and K. Chu, *Appl. Catal., B*, 2022, **316**, 121651.
49 N. Zhang, G. Zhang, P. Shen, H. Zhang, D. Ma and K. Chu, *Adv. Funct. Mater.*, 2023, DOI: **10.1002/adfm.202211537**.
50 G. Wang, P. Shen, K. Chen, Y.-L. Guo, X. Zhao and K. Chu, *Inorg. Chem. Front.*, 2023, DOI: **10.1039/d2qi02757g**.
51 K. Chen, Z. Ma, X. Li, J. Kang, D. Ma and K. Chu, *Adv. Funct. Mater.*, 2023, DOI: **10.1002/adfm.202209890**.
52 X. Li, P. Shen, Y. Luo, Y. Li, Y. Guo, H. Zhang and K. Chu, *Angew. Chem., Int. Ed.*, 2022, **134**, e202205923.
53 G. Wang, P. Shen, Y. Luo, X. Li, X. Li and K. Chu, *Dalton Trans.*, 2022, **51**, 9206–9212.
54 J. Shi, C. Wang, R. Yang, F. Chen, N. Meng, Y. Yu and B. Zhang, *Sci. China. Chem.*, 2021, **64**, 1493–1497.
55 X. Li, K. Chen, X. Lu, D. Ma and K. Chu, *Chem. Eng. J.*, 2023, **454**, 140333.
56 Y. Xu, K. Shi, T. Ren, H. Yu, K. Deng, X. Wang, Z. Wang, H. Wang and L. Wang, *Small*, 2022, **18**, 2203335.
57 T. Ren, Z. Yu, H. Yu, K. Deng, Z. Wang, X. Li, H. Wang, L. Wang and Y. Xu, *Appl. Catal., B*, 2022, **318**, 121805.
58 T. Ren, K. Ren, M. Wang, M. Liu, Z. Wang, H. Wang, X. Li, L. Wang and Y. Xu, *Chem. Eng. J.*, 2021, **426**, 130759.
59 D. Wu, P. Lv, J. Wu, B. He, X. Li, K. Chu, Y. Jia and D. Ma, *J. Mater. Chem. A*, 2023, **11**, 1817–1828.
60 B. He, P. Lv, D. Wu, X. Li, R. Zhu, K. Chu, D. Ma and Y. Jia, *J. Mater. Chem. A*, 2022, **10**, 18690–18700.
61 D. Wu, J. Wu, P. Lv, H. Li, K. Chu and D. Ma, *Small Struct.*, 2023, DOI: **10.1002/sstr.202200358**.
62 W. Zhang, M. Jiang, S. Yang, Y. Hu, B. Mu, Z. Tie and Z. Jin, *Nano Res. Energy*, 2022, **1**, e9120033.
63 K. Chu, Y. Luo, P. Shen, X. Li, Q. Li and Y. Guo, *Adv. Energy Mater.*, 2022, **12**, 2103022.
64 G. Zhang, X. Li, K. Chen, Y. Guo, D. Ma and K. Chu, *Angew. Chem., Int. Ed.*, 2023, DOI: **10.1002/anie.202300054**.
65 Y. Luo, K. Chen, G. Wang, G. Zhang, N. Zhang and K. Chu, *Inorg. Chem. Front.*, 2023, **10**, 1543–1551.
66 X. Li, P. Shen, X. Li, D. Ma and K. Chu, *ACS Nano*, 2023, **17**, 1081–1090.